communications earth & environment

ARTICLE

https://doi.org/10.1038/s43247-023-01032-9 OPEN

Atlantic inflow and low sea-ice cover in the Nordic Seas promoted Fennoscandian Ice Sheet growth during the Last Glacial Maximum

Margit H. Simon[1,2✉], Sunniva Rutledal[1,2,3], Laurie Menviel[4], Tobias Zolles[2,3], Haflidi Haflidason[2,3], Andreas Born[2,3], Sarah M. P. Berben[5] & Trond M. Dokken[1,2]

The Atlantic water inflow into the Nordic Seas has proven difficult to reconstruct for the Last Glacial Maximum. At that time, the Fennoscandian Ice Sheet grew potentially to its maximum extent. Sea-ice free conditions in the eastern Nordic Seas have been proposed as an essential moisture source contributing to this build-up. It has been hypothesized that the inflow of warm and saline Atlantic surface waters was important for maintaining these seasonally sea-ice free conditions in the Nordic Seas at that time. However, the difference between a perennially frozen ocean and a seasonally open ocean on ice sheet build-up remains unquantified. Here we use, tephra-constrained surface ventilation ages from a network of marine sediment cores and model experiments, to show that Atlantic inflow to the southern Nordic Seas likely occurred predominately via the Iceland-Faroe Atlantic inflow pathway helping to maintain seasonal open waters at the onset of the Last Glacial Maximum. Using a numerical snow model, we further demonstrate that such open-ocean conditions may have been a factor contributing to the Fennoscandian Ice Sheet growth with up to ~150% increase in surface mass balance over Norwegian coastal areas, compared to sea-ice covered conditions.

[1] Norwegian Research Centre (NORCE), Nygårdsgaten 112, 5008 Bergen, Norway. [2] Bjerknes Centre for Climate Research, Jahnebakken 5, 5007 Bergen, Norway. [3] Department of Earth Science, University of Bergen, 5007 Bergen, Norway. [4] Climate Change Research Centre, University of New South Wales, 2052 Sydney, NSW, Australia. [5] IMDC, Van Immerseelstraat 66, 2018 Antwerp, Belgium. ✉email: msim@norceresearch.no

To understand the mechanisms initiating and transmitting abrupt global climate change, precise reconstructions of past climates are essential. The high-latitude North Atlantic is a region of particular interest as climate changes there have global effects[1], especially through changes in the Atlantic Meridional Overturning Circulation (AMOC), which transports heat from low to high latitudes. During warm climate periods such as today, the AMOC is in a vigorous state, with active dense-water formation via open-ocean convection in the Nordic Seas[2–4] and the Labrador Sea[5]. This leads to the advection of warm and saline Atlantic surface waters into the Nordic Seas, enabling sea-ice free conditions in large parts of the Nordic Seas and a relatively warm climate in Western Europe[6]. This circulation pattern is currently maintained by a colder southward return flow at depth, formed through surface cooling processes and the sinking of dense waters in the Nordic Seas[7,8]. During past cold climate periods, such as the Last Glacial Maximum (LGM) (26.5–19 ka BP[9]), the strength and geometry of the AMOC are suggested to have been altered[10–12] and the Northern Hemisphere continental ice sheets expanded potentially to their maximum extent[13,14]. Changes in Nordic Seas sea surface conditions providing a potential moisture source supporting this build-up have been suggested before[15,16] but remain discussed[17]. Robust chronological control and reliable proxy methods are vital to confidently constrain the Nordic Seas sea-ice state and associated Atlantic water inflow dynamics at that time.

Previously, it was suggested that the LGM high-latitude North Atlantic and the Nordic Seas had a permanent sea ice cover[18]. Further, it was proposed that deep convection in the Nordic Seas was likely weak and unstable[19] or only occurred south of Iceland during the LGM[20]. Now the majority of evidence put forward suggests (at least) seasonally sea-ice free conditions in the Nordic Seas and active Atlantic water inflow east of Iceland, via the Faroe-Shetland Channel and/or over the Iceland-Faroe Ridge, at the onset and during the LGM[15,21–28]. This active Atlantic water inflow was maintained by a southern return flow at intermediate depths formed through convection in the Nordic Seas[23,29,30]. Additionally, it has been proposed that the Atlantic surface water in the Nordic Seas likely subducted and continued as a subsurface flow northward[31,32] due to increased seasonal meltwater input from surrounding ice sheets, which stratified the water column[23,24]. Despite progress in the field, the Nordic Seas remain a challenging region for climate reconstructions as large discrepancies between the different temperature and sea ice extent reconstructions exist[17,24] and absolute age control is problematic.

The difference between a perennially frozen ocean and an open or seasonally open ocean has wide climatic implications. The advection of warm and saline Atlantic surface water into the Nordic Seas increases evaporation and precipitation in the area. As such, it has been hypothesized that seasonally open eastern Nordic Seas during the LGM could have acted as an essential moisture source for the Fennoscandian Ice Sheet build-up, e.g., refs. [15,33,34]. However, more data with sufficient spatial coverage and robust age control is needed to demonstrate that there were seasonally open ocean conditions and what the quantitative implications of those were on the Fennoscandian ice sheet growth.

To explore this, we first investigate near-surface circulation changes at the onset of the LGM in the high-latitude North Atlantic by reconstructing near-surface (based on planktic foraminifera) marine ^{14}C reservoir ages (MRAs) from a spatial network of ten marine sediment cores. Nine of these cores are situated along the path of Atlantic surface currents entering the Nordic Seas and one is in the Irminger Sea (Figs. 1, 2 and Supplementary Fig. S1). MRAs are an established tool for

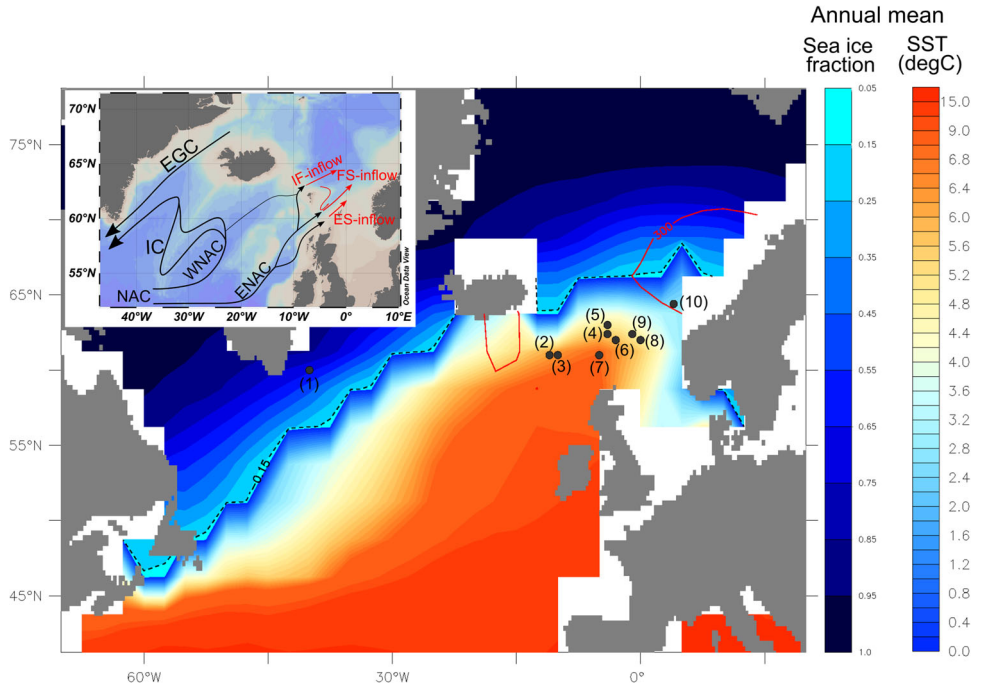

Fig. 1 Annual mean sea surface temperature (SST (°C)) and sea-ice fraction from the transient marine isotope stage (MIS) 3- MIS3 LOVECLIM simulation averaged over 26.7–26.6 ka BP. Black dashed contour refers to the 15% sea-ice edge. Red contours refer to 300 m mixed layer depth. This contour thus shows the location of deep-ocean convection. Black circles and numbers denote the locations of sediment cores included in the study. (1) GS16-204-18CC, (2) ENAM33, (3) ENAM30, (4) ENAM93-20, (5) ENAM93-21, (6) JM11-19PC, (7) LINK04, (8) LINK17 (9) MD99-2284, (10) MD99-2289. The inset map (generated using Ocean Data View[99]) shows the modern bathymetry with main surface water currents. EGC East Greenland Current, IC Irminger Current, NAC North Atlantic Current, WNAC Western North Atlantic Current, ENAC Eastern North Atlantic Current, IF- inflow Iceland - Shetland Atlantic inflow, FS-inflow Faroe – Shetland Atlantic inflow, ES- inflow European Shelf Atlantic inflow[40].

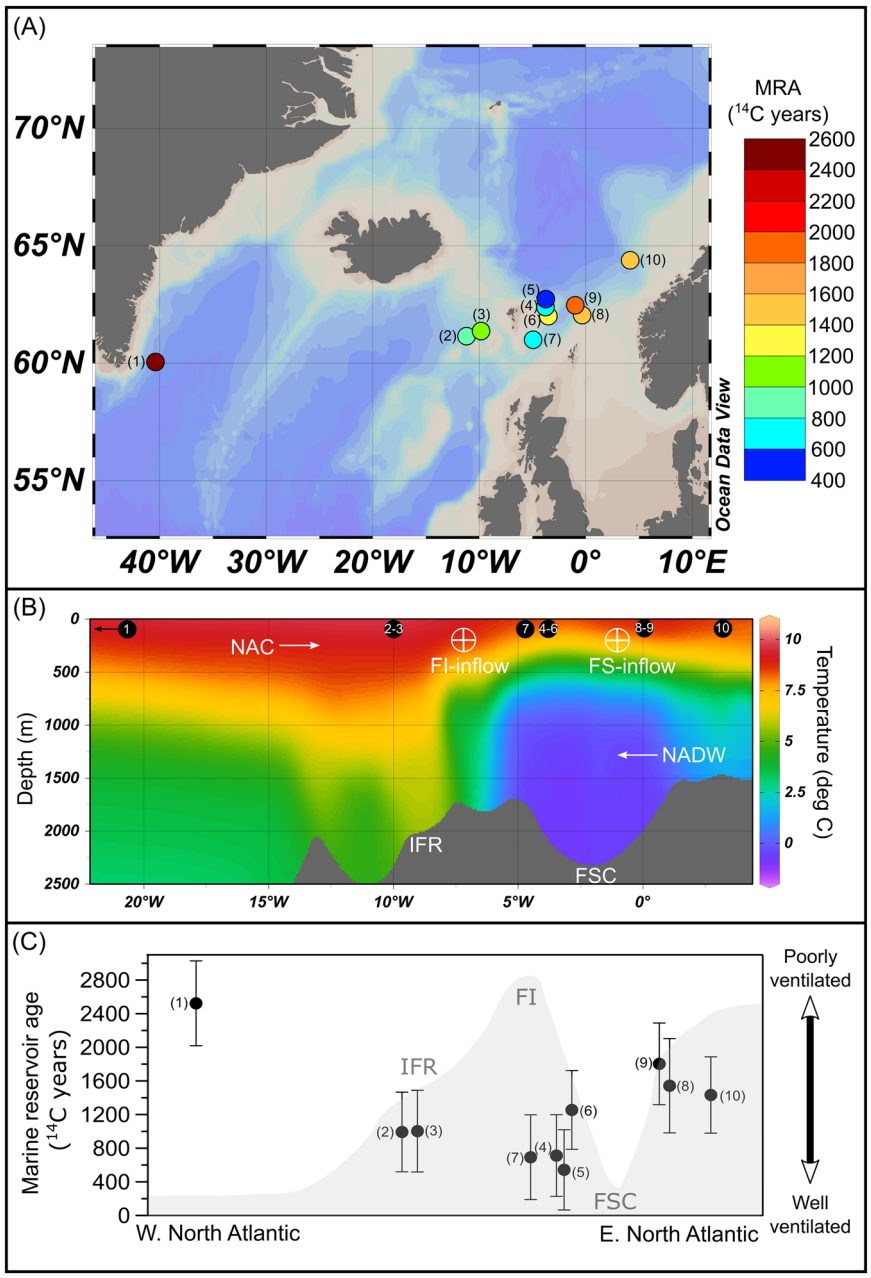

Fig. 2 Reconstructed near-surface marine reservoir ages (MRAs) in the high-latitude North Atlantic at 26 690 BP (i.e., FMAZ II-1 event). **A** Reconstructed MRAs plotted on the base map generated using the ODV software[99] sediment cores are numbered following Table S1. **B** West-east Atlantic depth transect showing the mean annual temperature (25° grid) for the 1955–2017 time period from the World Ocean Atlas 2018 database[100], the approximate position of *N. pachyderma* depth habitat for sediment core location is shown. Numbers follow Table S1. NAC North Atlantic Current, ENAC Eastern North Atlantic Current, WNAC Western North Atlantic Current, NADW North Atlantic Deep Water, IFR Iceland-Faroe Ridge, FSC Faroe-Shetland Channel., FI Faroe Islands. **C** Reconstructed MRAs. Sediment cores are numbered following Table S1. The background shading refers to the simplified east-west positioning of the sediment cores relative to the approximate bathymetry of the FSC and IFR. Error bars are calculated using the summation in quadrature method (see material and methods).

investigating past changes in the North Atlantic surface ocean circulation[35–37]. They reflect an offset between the ^{14}C concentration in the contemporaneous atmosphere and surface ocean[38,39].

Today warm and well-ventilated Atlantic waters originating from the tropics, enter the eastern Nordic Seas mainly via the eastern branch of the North Atlantic Current in three ways: (1) the Iceland–Faroe Atlantic inflow over the Iceland-Faroe Ridge, (2) the Faroe–Shetland Atlantic inflow within the Faroe-Shetland Channel, (3) the European Shelf Atlantic inflow between the southeastern boundary of the Faroe–Shetland Channel and the European continent[40,41] (Fig. 1, S1). Another path of warm and well-ventilated Atlantic waters is via the Irminger Current (IC) into the Irminger Sea, where the Polar Front separates it from cold and fresh Arctic origin waters carried by the East Greenland Current (EGC)[42] (Figs. 1, S1). Thus, the MRAs observed in the southern Nordic Seas today, of ~350–400 ^{14}C years (Fig. S2) are considered to reflect a modern surface ocean circulation pattern with Atlantic currents carrying recently equilibrated warm and saline surface waters northwards from the tropics to the high-

latitudes. Therefore, the identification of higher than modern surface MRAs during the Last Glacial period has been suggested to reflect a reduction in the Atlantic surface water inflow currents[43], potentially associated with reduced overturning circulation in the Nordic Seas[44]. Overall, this process would result in a decreased influence of relatively "young ^{14}C" tropical-sourced surface waters, and an increased influence of "old ^{14}C" polar-sourced waters[43].

To quantify MRAs, reliable non-radiometric-based time markers are essential. Here, we use tephrochronology, one of the most precise geochronological methods currently available, which has also proven successful in quantifying past MRAs[44–46]. As such, the Faroe Marine Ash Zone II, also called Fugloyarbanki (FMAZ II-1) tephra marker is of particular interest as its traces can be identified over a large geographical area in the high-latitude North Atlantic[47–49] and in the Greenland ice-core NGRIP[50]. Based on its occurrence in NGRIP, the FMAZ II-1 tephra event occurred 26 690 ± 390 years BP, which is perfectly positioned to constrain the onset of the LGM[51].

To assess the climatic conditions prevailing in the high-latitude North Atlantic as suggested by our proxy record at the onset of the LGM, we secondly quantify and characterize the Atlantic water inflow dynamics into the Nordic Seas associated with this climate background state, as simulated in a transient simulation performed with the Earth system model of intermediate complexity LOVECLIM[52]. Finally, to quantify the influence of Nordic Seas' sea-ice cover on Fennoscandian Ice Sheet growth we use the BErgen Snow SImulator (BESSI). This surface mass balance (SMB) model is used to compute the Fennoscandian Ice Sheet SMB in two different hypothesized scenarios where (i) the Nordic Seas are seasonally sea-ice free and (ii) the Nordic Seas are sea-ice covered, using the LOVECLIM simulation accordingly.

Hence, our study goes beyond previous work in that, for the first time to the best of our knowledge, we quantify the effect such different scenarios would have on the Fennoscandian ice-sheet SMB.

Results

Surface ocean ventilation changes in the high-latitude North Atlantic at the onset of the LGM. Figure 2 displays the reconstructed variability in near-surface MRAs from ten marine sediment cores included in this study. The results indicate that at the onset of the LGM, higher than modern near-surface MRAs occurred in both the Irminger Sea, site 1 (2523 ± 504 ^{14}C years, Fig. 2A, C, Supplementary Table S1) and in the Norwegian Sea, east of Faroe-Shetland Channel sites 8–10, (1433 ± 453 to 1803 ± 485 ^{14}C years, Fig. 2, Table S1)[43]. MRAs west of the Faroe-Shetland Channel (sites 2–7) were lower than found elsewhere (543 ± 477 to 1003 ± 485 ^{14}C years, Fig. 2A, C, Table S1). An exception in this group is site 6 (JM11-19PC) with a higher MRA of 1255 ± 468 ^{14}C years. These results point towards regional differences in MRAs around the Faroe-Shetland Channel, where older ages are found on the eastern side (Fig. 2A, C) along the Faroe–Shetland Atlantic inflow pathway.

Simulated high-latitude North Atlantic circulation changes and sea-ice state at the onset of the LGM. To quantitatively address the state of the Nordic Seas sea-ice cover and the Atlantic surface water inflow dynamics into the Nordic Seas, we explore the model outputs from a transient experiment of the Last Glacial period performed with the LOVECLIM Earth system model of intermediate complexity[52,53]. After an equilibration under 50 ka BP boundary conditions, the model is forced by the time-varying evolution of insolation (calculated from the orbital parameters[54]), Northern Hemisphere ice-sheet topography, and albedo[55], and atmospheric CO_2 concentration[56]. To mimic the Dansgaard-Oeschger variability of the Last Glacial period, the buoyancy of the North Atlantic region (55°W–10°W, 50°N–65°N) is modulated so that the simulated sea-surface temperatures (SSTs) off the Iberian margin are in relative agreement with paleo-proxy estimates[52,57,58]. During the period of interest here (i.e., at the onset of the LGM, ~ 27–25 ka BP), the model is forced by a meltwater input in the North Atlantic of 0.06 Sv between 26.9 and 25.7 ka BP (Fig. S3). As a result, the AMOC strength is ~13.4 Sv at 26.7 ka BP, compared to ~25 Sv for the pre-industrial (PI) control run. Under glacial boundary conditions, in this version of the model, the Labrador and Irminger Seas are covered by sea-ice, therefore inhibiting deep-water formation in that region[10]. At 26.7 ka BP, North Atlantic deep-water (NADW) is thus primarily formed in the Nordic Seas between 65°N and 70°N, which corresponds to the annual mean sea-ice edge, while a minor component of NADW is formed south of Iceland (Fig. 1). When the mixed layer depth is deeper than 300 m, there is deep-ocean convection in the model.

Due to the presence of a large Laurentide Ice Sheet at that time, the North Atlantic wind stress is ~18% stronger and slightly shifted to the south. In addition, the wind stress associated with the polar easterlies is also stronger. Combined, this results in a 30% stronger and eastward shifted subpolar gyre (SPG) at 26.7 ka BP compared to the PI control run (Fig. 3). These combined changes in SPG and deep-water formation lead to a northward transport of Atlantic-sourced waters of 6.6 Sv into the Nordic Seas which occurs east of Iceland. The equivalent ocean heat transport at 64°N is 131 TW. In comparison, the volume and heat transport for the PI control run is 7.4 Sv and 262.6 TW, which compares relatively well to modern oceanographic estimates[59]. Furthermore, due to changes in the oceanic circulation pattern and associated deep-water formation, the ocean-to-atmosphere heat flux is centered in the southern Nordic Seas and the northeast Atlantic (55°N–70°N, 30°W–10°E) at 26.7 ka BP. The integrated ocean-to-atmosphere heat flux in the North Atlantic (north of 56°N) is reduced by 32% from a magnitude of 433 TW during the PI control run (Fig. 3). As a result, while evaporation is reduced over most of the North Atlantic region, it increases over a small region of the northeastern Atlantic/southern Nordic Seas (50°N–65°N, 25°W–0°) (Fig. S4), which contributes to the moisture supply towards the Fennoscandian Ice Sheet. Precipitation over Scandinavia is only 12% weaker at 26.7 ka BP compared to the PI control run (Fig. S4).

As this transient experiment did not include radiocarbon, a direct MRA model-data comparison cannot be shown. However, results of a previously published radiocarbon-isotope-enabled LGM experiment using LOVECLIM can be used. This model run features an oceanic circulation similar to the one presented here[60] (AMOC of 14.7 Sv). Overall, we find that the simulated LGM MRAs in the Faroe-Shetland Channel are about 150 ^{14}C years higher than the simulated PI ages (Fig. S5). This is in relative agreement with the reconstructed results from cores 4, 5, and 7 located west in the channel, but at odds with cores 8–10 located east and north of the channel (more information can be found in the Supplementary Materials).

Contributions of the Nordic Seas sea-ice state on continental ice sheet growth. To address the potential influence of the Nordic Seas' sea-ice cover on Fennoscandian Ice Sheet growth, we performed two model runs with the surface energy and mass balance model BESSI[61,62], forced by output data from the LOVECLIM simulation. One way to do so is by comparing two very contrasting scenarios: a perennially frozen ocean and an open or seasonally open one. Therefore, in the first experiment, we use the

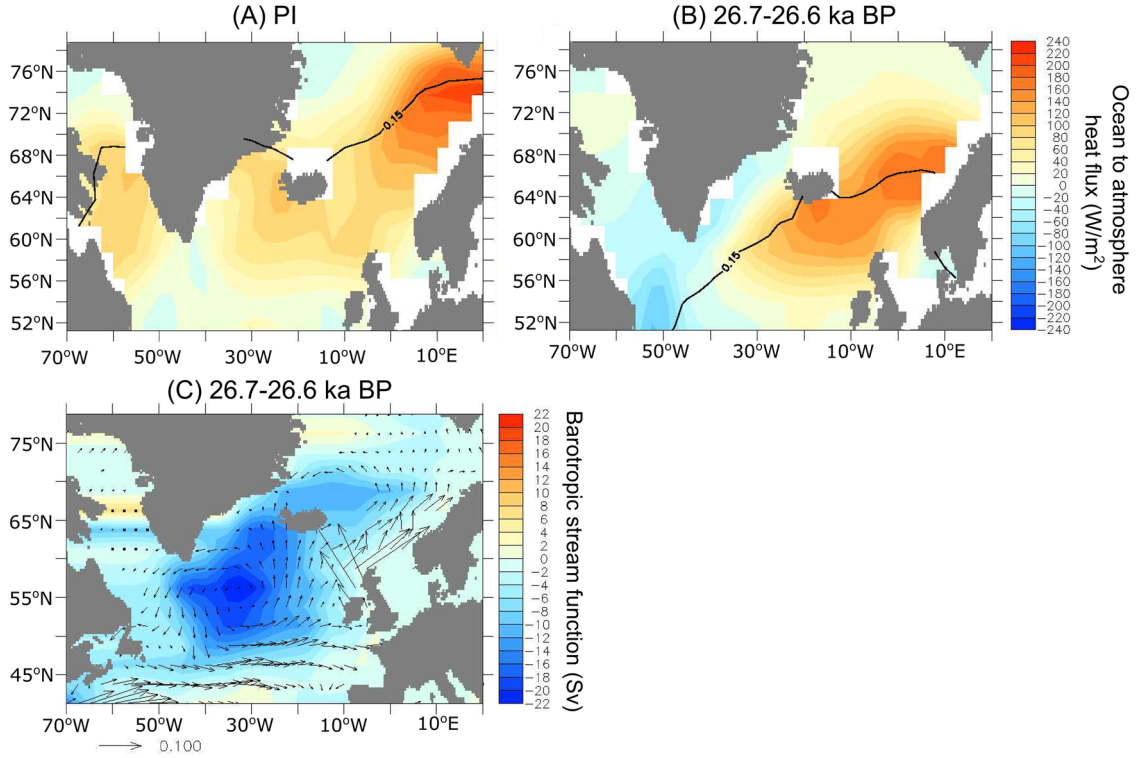

Fig. 3 Annual mean ocean to atmosphere heat flux (W/m^2) and barotropic stream function (Sv). A Pre-Industrial annual mean ocean to atmosphere heat flux (W/m^2). The 0.15 isoline shows the contour of the annual 15% sea-ice concentration (**B**) 27.7–26.6 ka BP annual mean ocean to atmosphere heat flux (W/m^2). **C** 26.7–26.6 ka BP barotropic stream function (Sv) with 0–106 m currents overlaid.

outputs presented earlier, corresponding to 26.7 ka BP, with an active, but relatively weak AMOC (~13.4 Sv, red dashed vertical box in Fig. S3) and seasonally sea-ice free Nordic Seas. This experiment is compared to a 24.9 ka BP state, where the AMOC is off (black vertical line in Fig. S3) and the Nordic Seas are completely sea-ice covered. The BESSI simulations show continental ice growth over Greenland, Iceland, Scandinavia, Scotland, and the Alps for both AMOC states (i.e., AMOC ~ 13.4 Sv and AMOC off) (Fig. 4A, B). However, compared to the AMOC off simulation, in the AMOC on scenario, the growth of the Fennoscandian Ice Sheet is more substantial, in particular, along the Norwegian coast and further north, where an increase of up to 150% in the SMB is recorded (Fig. 4C, D). A 50% SMB increase is also simulated over present-day Finland and the north coast of Poland.

Discussion

Reconstructed ventilation age patterns suggest active Atlantic water advection into the southern Nordic Seas. The modern-day MRAs in the regions of interest are on average 100–150 ^{14}C years (Fig. S2) younger than the global mean of approx. 500 ^{14}C years[63]. However, due to lower CO_2 partial pressure during the LGM, the surface ocean reservoir ages are expected to be globally approx. 250 years older than today[64]. Thus, we can expect that near-surface MRA values of ~600–650 ^{14}C years at the onset of the LGM indicate near-surface ocean conditions similar to the present day in the Nordic Seas. Other lines of evidence suggest that in the modern Arctic Ocean which is mostly sea-ice covered and highly stratified, MRAs average around 600–800 ^{14}C years[65,66], which when corrected for LGM conditions amounts to approximately 850–1050 ^{14}C years.

A striking observation from the reconstructed data is the large difference in near-surface MRAs along sites situated west (sites 2–7) and east of the Faroe Shetland Channel (sites 8–10) (Fig. 2).

First, we consider if the here identified spatial variability in marine radiocarbon ages at the onset of the LGM can also be recognized in the modern Nordic Seas. Today, the range of radiocarbon ages is up to ~200 ^{14}C years (averaging between 100–150 ^{14}C years) younger than the mean global ocean values, e.g., refs. [67,68] (Fig. S2). The differences in reconstructed near-surface MRAs between sites east and west of the Faroe-Shetland Channel greatly exceed this modern regional variability of ~200 ^{14}C (Fig. 2, Table S1). Hence, the higher than modern MRAs (~600–650 ^{14}C) at the onset of the LGM found east of the Faroe-Shetland Channel (sites 8–10) (1433 ± 453 to 1803 ± 485 ^{14}C years) and in the Irminger Sea, site 1 (2523 ± 504 ^{14}C years, Fig. 2A, C, Table S1) can be interpreted to represent a reduction in the influence of Atlantic surface waters at that time. Conversely, the ages found west of the Faroe-Shetland Channel (sites 2–7) are closer to a modern-day range within error margins (543 ± 477 to 1003 ± 485 ^{14}C years) and thus point to a maintained, however still likely weaker than modern NAC inflow to the southern Nordic Seas (Figs. 1–2). This suggests that the eastern branch, the Faroe-Shetland Atlantic- and European Shelf Atlantic inflow, was likely reduced and the main inflow geometry shifted to the western side, the Iceland-Faroe Atlantic inflow branch, which then acted as the main pathway for heat and salt to reach the higher latitudes.

We cannot completely rule out that the sites east of the Faroe-Shetland Channel (sites 8–10) are also influenced by secondary processes, despite circulation changes, limiting the ocean-atmosphere ^{14}C exchange. Processes that would drive the ventilation ages to higher ages include potentially increased sea-ice cover along the shelf, meltwater input, and upwelling of poorly ventilated waters to the surface associated with polynya formation that resulted from katabatic winds blowing seaward of the ice

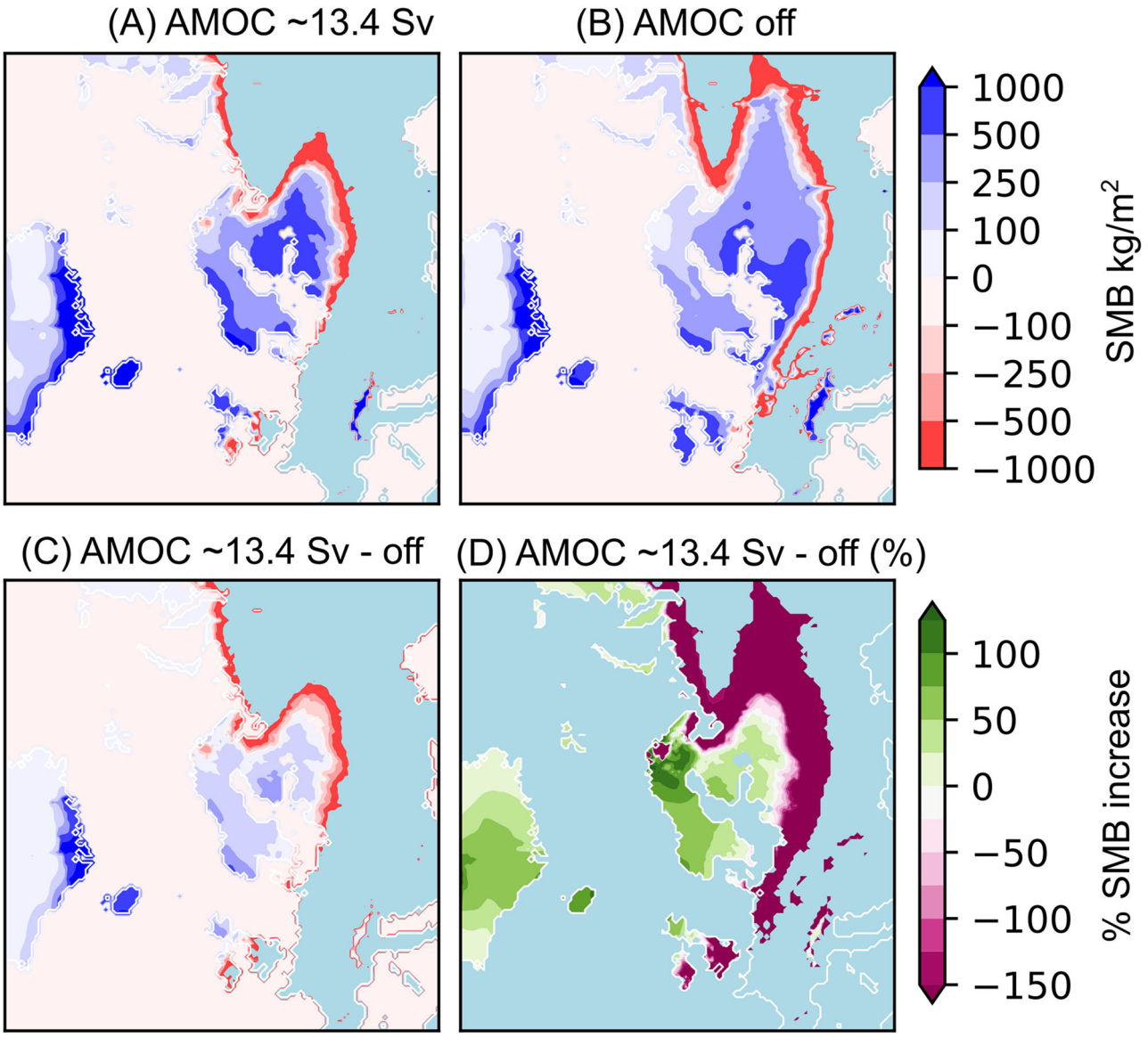

Fig. 4 Modeled surface mass balance SMB over the Fennoscandian Ice Sheet. A SMB for Atlantic Meridional Overturning Circulation (AMOC) ~ 13.4 Sv scenario with Nordic Seas' sea-ice free conditions as depicted by the LOVECLIM simulation averaged over 26.7–26.6 ka BP. **B** SMB for AMOC off scenario with Nordic Seas perennially sea-ice covered. **C** The difference in SMB between AMOC ~ 13.4 Sv and AMOC off run. **D** % SMB increase for AMOC ~ 13.4 Sv run compared to AMOC off run.

shelves e.g., refs. [15,33,34]. Nevertheless, we interpret our proxy results to indicate that the main pathway of Atlantic near-surface water entering the Nordic Seas occurred predominately via the Iceland- Faroe Atlantic inflow pathway. This is in agreement with findings from Rasmussen and Thomsen[28] in which, based on foraminiferal abundances and stable isotope work, it was shown that the warm Atlantic surface water pushed northward into the Nordic seas both east and west of the Faroe Islands during the LGM.

We further validate this interpretation with our LOVECLIM simulation at 26.7 ka BP, which features an active Atlantic inflow (6.6 Sv) into the Nordic Seas, occurring east of Iceland (Fig. 1). Additionally, the FMAZ II-1 tephra marker is interpreted to be a primary tephra deposit (i.e., homogenous geochemistry)[49] which was near-instantaneously deposited on the sea floor either through primary air-fall or by rafting of seasonal sea-ice (Table S1). Based on the homogenous tephra evidence alone, all core sites must have been either seasonally sea-ice free or at least close to seasonally sea-ice free areas at the time of the FMAZ II-1 volcanic eruption (i.e., at the onset of the LGM).[15,21–28]. The latter agrees with the LOVECLIM transient experiment at 26.7 ka BP, which also suggests seasonally sea-ice free conditions in the eastern Nordic Seas (Fig. 1). Nevertheless, the authors acknowledge the need for additional sea-ice proxy evidence such as IP25 (a highly branched isoprenoid lipid biomarker) to conclude on the presented hypothesis.

In the Irminger Sea, we find the oldest near-surface MRA (2523 ± 504 ^{14}C years) of the study (Fig. 2), suggesting that surface waters were isolated from the atmosphere during most of the year. The implied ocean conditions are in line with and validate the scenario from the LOVECLIM model simulation, which indicates the reduced influence of Atlantic-sourced waters and a greater sea-ice cover in that area at the onset of the LGM (Fig. 1). Based on the model simulation this region is fully covered by sea-ice, therefore inhibiting deep-ocean convection in the Labrador Sea region[10]. These conditions can be explained by a stronger EGC, which increases the freshwater input to the region and suppresses deep-ocean convection in the Labrador Sea[69].

Arctic-sourced, fresh surface waters have an older ^{14}C age signature[70] compared to Atlantic-sourced surface waters. A stronger EGC coupled with sea-ice cover and a cessation of deep-ocean convection in the Labrador Sea would explain the poorly ventilated near-surface ocean signature in the Irminger Sea at the onset of the LGM (Figs. 1–3).

Mechanisms controlling the advection of Atlantic waters into the Nordic Seas at the onset of the LGM. Today, the inflow of warm and saline Atlantic water into the Nordic Seas is modulated by several processes such as the strength of the AMOC[71], the intensity and strength of the North Atlantic SPG[72,73], and North Atlantic wind stress[74,75]. A stronger North Atlantic wind stress increases the barotropic flow component which strengthens the SPG[76]. Furthermore, a strong SPG would enhance the influence of fresher waters drawn from the western SPG region, which reduces the export of saline waters from the subtropical gyre (STG)[77]. Building on modern observations, this reduces the strength of Atlantic water inflow, in terms of heat and volume transport, into the Nordic Seas[72,78], as less saline and warm STG waters become entrained in the northward inflow[72]. The LOVECLIM simulation at 26.7 ka BP presented here suggests such a scenario. Due to the presence of a large Laurentide Ice Sheet, the North Atlantic wind stress was slightly shifted south and stronger, in good agreement with more comprehensive models[76,79,80]. As a result, the SPG extended eastwards and was ~30% stronger (Fig. 3C). Comparable to modern observations[72], the simulated stronger SPG at the onset of the LGM forces a reduction in the Nordic Seas Atlantic water inflow, of ~12% in volume (Sv) and ~50% in heat (TW) transport compared to the PI control run. Despite the reduction in the northward Atlantic inflow, a substantial amount of heat (131 TW) is still transported into the Nordic Seas, which helps maintain active deep-ocean convection centered in the southern Nordic Seas, corresponding to the annual mean sea-ice edge (65–70°N) (Fig. 3). Collectively, these processes lead to seasonally sea-ice free conditions in the southern Nordic Seas at 26.7 ka BP.

Taken together, the proxy data and numerical model simulation suggest that the southeastern Nordic Seas were seasonally sea-ice free with an active, but weaker, inflow of Atlantic waters occurring east of Iceland at the onset of the LGM.

Nordic Seas: an important moisture source for Fennoscandian Ice sheet build-up at the onset of LGM. At the onset of the LGM (~27–26 ka BP), the British Isles Ice Sheet and the Fennoscandian Ice Sheet grew so that the westernmost limits along the British-Irish and Norwegian continental shelf were reached[13]. Such an extensive growth of large continental ice sheets required a substantial moisture supply. The BESSI model results show that under seasonally sea-ice free conditions in the Nordic Seas and with an AMOC strength of ~13.4 Sv as depicted by the LOVECLIM 26.7 ka BP simulation, the snowfall increased by up to 150% over the Fennoscandian Ice Sheet (Figs. S6, S7), compared to when the Nordic Seas are sea-ice covered (i.e., AMOC off). Thus, the Fennoscandian Ice Sheet SMB benefits more from the additional moisture from the sea ice-free ocean surface than it is impacted by the simultaneously rising air temperatures. Particularly, the Norwegian coastal regions are most affected by sea-ice free conditions in the Nordic Seas in terms of increased snowfall and positive SMB (Fig. 4, Fig. S7). In regions further south, such as over the southern British Isles Ice Sheet, sea-ice free conditions have a negative impact on the SMB. This is due to a reduced snowfall increase, which is not able to compensate for the warmer temperatures in these regions (Figs. S6, S7). Combined, our results demonstrate the importance of the Nordic Seas sea surface conditions for the Fennoscandian Ice Sheet build-up at the onset of the LGM.

Conclusions

Our findings, taken together with existing studies on LGM Nordic Seas sea surface conditions[15,21–28,81] suggest near-surface Atlantic water advection into the Nordic Seas and likely seasonally sea-ice free conditions at the onset of the LGM. Active Atlantic water advection under glacial boundary conditions propagating from south of the Greenland-Scotland Ridge in the North Atlantic, into the Nordic Seas (east of Iceland) and northwards to at least 65–70°N is therefore now demonstrated by proxy and model data (Fig. 1). Ultimately, these oceanic conditions were potentially one important factor contributing to Fennoscandian Ice Sheet growth, in particular over northern and coastal Norway. This study only presents a "snapshot" of the ocean circulation changes at the onset of the LGM. More work is needed to produce a spatial network of ocean circulation- and sea ice changes over time to quantify the impact of ocean moisture source areas on northern high-latitude ice sheets in the past. Multi-model ensembles may be used in the future to better decipher the variety of factors contributing to Northern Hemisphere ice sheet growth.

Materials and methods

Tephra analysis and Accelerator Mass Spectrometry (AMS) ^{14}C dates. Tephra analysis from all ten marine sediment cores as well as eight AMS ^{14}C dates are already published and the data is available (Table S1). Sedimentation rates of the core used in this study together with their marine reservoir ages are shown in Fig. S9. Available paleoproxy data from selected sediment cores used in the study is demonstrated in S10.

Here, we add radiocarbon dates to the existing ones from two key sites in the high-latitude North Atlantic Ocean: offshore southeast Greenland (GS16-204-18CC) (site 1) and the southern Norwegian Sea (MD99-2284) (site 9). For the near-surface MRA reconstruction, approximately 1.5 mg of planktic foraminifera specimens (150–500 µm) in pristine condition were picked from the same depth level as the identified FMAZ II-1 tephra marker. The samples were then radiocarbon-dated using AMS ^{14}C measurement procedures at ETH Zürich, Switzerland. There, the samples were processed using a newly developed method[82] involving direct CO_2 measurements of ~0.5 mg using an AMS facility equipped with a gas ion source. In addition, we performed leaching experiments on the sample surface material using HCl 0.02 M, following procedures in ref. [83]. The AMS ^{14}C dates from all sites were measured on the near-surface planktonic species *Neogloboquadrina pachyderma* (*N. pachyderma*) (calcification depth ~30–200 m[84,85]) permitting reconstruction of near-surface water mass properties. New plankton tow data[85] supports this interpretation demonstrating that the depth habitat of *N. pachyderma* varies between 25 and 280 m (average ~100 m). The study shows that sea-ice and chlorophyll concentrations at the surface, in combination with the time since the sea-ice break-up, explain almost a third of the variance in the depth habitat data[85].

We calculated the near-surface MRAs (in ^{14}C years) as the difference between the measured planktonic (*N. pachyderma*) ^{14}C age and the IntCal20 atmospheric ^{14}C calibration curve[86]. The uncertainty of the reconstructed MRAs is calculated by combining the uncertainty (summation in quadrature method) related to (1) ^{14}C analytical error, (2) GICC05 ice core age model error for FMAZ II-1 age, (3) IntCal20 calibration curve, and (4) transfer-function related to IntCal20 and GICC05 age offset[87]. For two of the marine sediment cores (no. 7 and 10), the AMS ^{14}C date was not extracted from the exact same core depth as the FMAZ II-1

tephra layer (Table S1). For sediment core LINK04 (site 7), the spacing between the AMS ^{14}C date and the position of the FMAZ II-1 tephra layer is 12 cm. Therefore, the AMS ^{14}C date was adjusted using the correction originally provided by ref. [48] (Table S1).

IntCal20 and GICC05 offset. The independent absolute age of the FMAZ II-1 tephra event is derived from the GICC05 ice-core chronology[51]. However, to estimate the MRA we compare the radiocarbon concentration of the near-surface ocean to the contemporaneous atmosphere, which is on a different age scale, the IntCal20. Ref. [87] identified systematic discrepancies between the precursor of IntCal20 (i.e., IntCal13 curve) and the GICC05 curve. At the time of the FMAZ II-1 event, ref. [87] estimates that the GICC05 chronology is about 445 ± 190 years younger than the IntCal13 chronology based on synchronizing the ice-core record to different ^{14}C datasets incorporated in IntCal13. The transfer function developed by ref. [87] to correct for this offset is still recommended for the IntCal20 curve[88]. As the tephra-based chronology follows GICC05 timescales, we report MRAs that have been corrected for this (Table S1) using the transfer function by ref. [87].

MRA calculation.

$$\begin{aligned} Atmospheric\ ^{14}C\ age &= Absolute\ age + \text{ref. (87) time} \\ &\quad - \text{scale offset} \rightarrow {}^{14}C\ age\ (IntCal20)\ MRA \\ &= N.pachyderma\ ^{14}C\ age - Atmospheric\ ^{14}C\ age \end{aligned} \quad (1)$$

The climate model: LOVECLIM. We present the results of a transient simulation of the last 50,000 years performed with the Earth System model of intermediate complexity, LOVECLIM[53]. LOVECLIM includes a free-surface ocean general circulation model with a horizontal resolution of 3degx3deg and 20 uneven vertical levels, coupled to a thermodynamic sea-ice model[89]. The atmospheric model is a global spectral T21 model, with 3 vertical levels, based on quasi-geostrophic equations of motion and ageostrophic corrections[90]. LOVECLIM also includes a land cover and terrestrial carbon model[91] as well as a marine carbon cycle model[92,93]. In this simulation of MIS 2, the only adjustment to the land-sea mask that was made was to close the Bering Strait.

Experimental setup. The transient simulation presented here is the continuation of the transient simulation of MIS 3 presented in ref. [52].

The model was equilibrated under 50 ka BP boundary conditions and then run transiently from 50 ka BP to 20 ka BP with appropriate boundary forcing: i.e., transient changes in orbital parameters[54], greenhouse gases, northern hemispheric ice-sheet orography and albedo[55]. The orbital parameters are calculated by the model with a yearly time step. The greenhouse gases vary yearly based on a linear interpolation of the data. The ice-sheet orography and albedo were obtained from an off-line ice-sheet model simulation[55] and are updated every 200 years. Episodic meltwater inputs into the North Atlantic[52] are also included to represent the millennial-scale variability of the last glacial period (Fig. S3A)[52]. Episodic meltwater inputs affect the strength of the AMOC, which varies between 0 and 40 Sv between 29 ka BP and 20 ka BP (Fig. S3B). The MRA data at ~26.7 ka BP suggest ocean conditions that are in line with a relatively weak AMOC, (i.e., ~13 Sv). Such an AMOC state was also inferred from an extensive model-data comparison of the LGM[10,60]. To appropriately assess the state of the Nordic Seas, the model outputs from 26.7 ka BP to 26.6 ka BP are thus studied here (red line in Fig. S3). To test the impact of seasonal ice-free conditions in the Nordic Seas on the Fennoscandian Ice Sheet build-up under boundary conditions similar to 26.7–26.6 ka BP, we use an alternate simulation, which featured a shutdown of the AMOC at 25 ka BP (black line in Fig. S3).

Model performances limitations. The performances of LOVECLIM are detailed in ref. [53]. For modern-day climate, the model reproduces well the main features of the temperature and precipitation distributions as well as the large-scale structure of the near-surface circulation. At low latitudes, the main biases are a 25 degC isotherm being located too far away from the equator and a precipitation distribution that is too symmetric between the hemispheres. The zero-degree isotherm is, however, quite close to the observed one in both hemispheres and the sea-ice cover is also relatively well represented in both hemispheres, even if the seasonal cycle in the North Atlantic is too weak.

The atmospheric model of LOVECLIM is based on quasi-geostrophic approximations but includes parametrizations of ageostrophic terms to better capture tropical dynamics. As such, some tropical modes of variability, such as the El Nino Southern Oscillation (ENSO) are not represented. However, given that the focus of this study is on a better understanding of the mean climate state during MIS3 at high northern latitudes, the lack of representation of tropical variability should not significantly impact the results.

BErgen Snow SImulator (BESSI) experimental design and limitations. The SMB simulations for the Fennoscandian Ice Sheet are conducted with the model BESSI[61]. BESSI is run with a 40 km resolution over the northern hemisphere, for 500 years using input from two LOVECLIM simulations: one simulation with open ocean conditions at 26.7 ka BP (i.e., AMOC on, strength ~13.4 Sv) and one simulation with a perennial sea-ice cover (i.e., AMOC off) around the Norwegian coast (AMOC off). BESSI requires daily input fields of surface air temperature, precipitation, short- and long-wave downward radiation at the surface, and humidity. All variables are interpolated bilinearly onto the 40 km grid (Fig. S8). Since suitable fields for radiation are not available from LOVECLIM, we use CCSM4 radiation forcing[94], which previous simulations have shown to keep the error below 5%. The LOVECLIM fields for precipitation and air temperature are bias-corrected with modern reanalysis (ERA-interim) data[95], using a simple additive bias for temperature and removing a multiplicative bias in the case of precipitation to avoid negative values. This method is described in detail in ref. [96]. In addition, BESSI downscales the temperature vertically to the more finely resolved topography of its own grid and corrects the longwave-radiation input with the thus modified temperature data. Two different lapse rates of 0.00065 and 0.0008 K/m were tested but led to similar qualitative results, so we include only the former[94,97]. Due to the simple topography in the LOVECLIM model, orographic precipitation is underestimated. To a certain degree, this can be solved via the bias correction used for the simulations presented here.

Data availability

The radiocarbon data generated in this study and the derived MRA estimates are available in the Supplementary Information in Table S1 and in the SEANOE repository[98].

Received: 14 July 2022; Accepted: 29 September 2023;
Published online: 21 October 2023

References

1. Voelker, A. H. L. Global distribution of centennial-scale records for Marine Isotope Stage (MIS) 3: a database. *Quat. Sci. Rev.* **21**, 1185–1212 (2002).
2. Marshall, J. & Schott, F. Open-ocean convection: observations, theory, and models. *Rev. Geophys.* **37**, 1–64 (1999).
3. Brakstad, A., Gebbie, G., Våge, K., Jeansson, E. & Ólafsdóttir, S. R. Formation and pathways of dense water in the Nordic Seas based on a regional inversion. *Prog. Oceanogr.* **212**, 102981 (2023).
4. Petit, T., Lozier, M. S., Josey, S. A. & Cunningham, S. A. Atlantic deep water formation occurs primarily in the Iceland basin and Irminger Sea by local Buoyancy forcing. *Geophys. Res. Lett.* **47**, e2020GL091028 (2020).
5. Feucher, C., Garcia-Quintana, Y., Yashayaev, I., Hu, X. & Myers, P. G. Labrador Sea Water formation rate and its impact on the local Meridional Overturning Circulation. *J. Geophys. Res. Oceans* **124**, 5654–5670 (2019).
6. Buckley, M. W. & Marshall, J. Observations, inferences, and mechanisms of the Atlantic Meridional Overturning Circulation: a review. *Rev. Geophys.* **54**, 5–63 (2016).
7. Hansen, B. & Østerhus, S. North Atlantic–Nordic Seas exchanges. *Prog. Oceanogr.* **45**, 109–208 (2000).
8. Srokosz, M. A. & Bryden, H. L. Observing the Atlantic Meridional Overturning Circulation yields a decade of inevitable surprises. *Science* **348**, 1255575 (2015).
9. Clark, P. U. et al. The Last Glacial Maximum. *Science* **325**, 710–714 (2009).
10. Menviel, L. C. et al. Enhanced Mid-depth Southward Transport in the Northeast Atlantic at the Last Glacial Maximum Despite a Weaker AMOC. *Paleoceanogr. Paleoclimatol.* **35**. https://doi.org/10.1029/2019PA003793 (2020).
11. Howe, J. N. W. et al. North Atlantic deep water production during the Last Glacial Maximum. *Nat. Commun.* **7**, 11765 (2016).
12. Kageyama, M. et al. The PMIP4 Last Glacial Maximum experiments: preliminary results and comparison with the PMIP3 simulations. *Clim. Past* **17**, 1065–1089 (2021).
13. Hughes, A. L. C., Gyllencreutz, R., Lohne, Ø. S., Mangerud, J. & Svendsen, J.-I. The last Eurasian Ice Sheets—a chronological database and time-slice reconstruction. https://doi.org/10.1111/bor.12142 (2016).
14. Batchelor, C. L. et al. The configuration of Northern Hemisphere ice sheets through the Quaternary. *Nat. Commun.* **10**, 3713 (2019).
15. Hebbeln, D., Dokken, T., Andersen, E. S., Hald, M. & Elverhøi, A. Moisture supply for northern ice-sheet growth during the Last Glacial Maximum. *Nature* **370**, 357–360 (1994).
16. Ruddiman, W. F. & McIntyre, A. Warmth of the Subpolar North Atlantic Ocean During Northern Hemisphere Ice-Sheet Growth. *Science* **204**, 173–175 (1979).
17. Paul, A., Mulitza, S., Stein, R. & Werner, M. A global climatology of the ocean surface during the Last Glacial Maximum mapped on a regular grid. *Clim. Past* **17**, 805–824 (2021).
18. CLIMAP. Seasonal reconstructions of the Earth's surface at the Last Glacial Maximum. *Geol. Soc. Am. Map Chart Series* **38**, 18 (1981).
19. Rasmussen, T. L. et al. The Faroe–Shetland Gateway: Late Quaternary water mass exchange between the Nordic seas and the northeastern Atlantic. *Marine Geol.* **188**, 165–192 (2002).
20. Boyle, E. A. & Keigwin, L. North Atlantic thermohaline circulation during the past 20,000 years linked to high-latitude surface temperature. *Nature* **330**, 35–40 (1987).
21. Oppo, D. & Lehman, S. J. Mid-depth circulation of the subpolar North-Atlantic during the Last Glacial Maximum. *Science* **259**, 1148–1152 (1993).
22. Raymo, M. E. et al. Stability of North Atlantic water masses in face of pronounced climate variability during the Pleistocene. *Paleoceanography* **19**. https://doi.org/10.1029/2003PA000921 (2004).
23. Meland, M. Y., Jansen, E. & Elderfield, H. Constraints on SST estimates for the northern North Atlantic/Nordic Seas during the LGM. *Quat. Sci. Rev.* **24**, 835–852 (2005).
24. de Vernal, A. et al. Comparing proxies for the reconstruction of LGM sea-surface conditions in the northern North Atlantic. *Quat. Sci. Rev.* **25**, 2820 (2006).
25. Waelbroeck, C. et al. Constraints on the magnitude and patterns of ocean cooling at the Last Glacial Maximum. *Nat. Geosci.* **2**, 127–132 (2009).
26. Veum, T., Jansen, E., Arnold, M., Beyer, I. & Duplessy, J.-C. Water mass exchange between the North Atlantic and the Norwegian Sea during the past 28,000 years. *Nature* **356**, 783–785 (1992).
27. Pflaumann, U. et al. Glacial North Atlantic: sea-surface conditions reconstructed by GLAMAP 2000. *Paleoceanography* **18**. https://doi.org/10.1029/2002PA000774 (2003).
28. Rasmussen, T. L. & Thomsen, E. Warm Atlantic surface water inflow to the Nordic seas 34-10 calibrated ka B.P: ATLANTIC SURFACE WATER INFLOW. *Paleoceanography* **23**, n/a (2008).
29. Crocket, K. C., Vance, D., Gutjahr, M., Foster, G. L. & Richards, D. A. Persistent Nordic deep-water overflow to the glacial North Atlantic. *Geology (Boulder)* **39**, 515–518 (2011).
30. Larkin, C. S. et al. Active Nordic Seas deep-water formation during the last glacial maximum. *Nat. Geosci.* **15**, 925–931 (2022).
31. Rasmussen, T. L., Pearce, C., Andresen, K. J., Nielsen, T. & Seidenkrantz, M.-S. Northeast Greenland: ice-free shelf edge at 79.4°N around the Last Glacial Maximum 25.5–17.5 ka. *Boreas* **51**, 759–775 (2022).
32. Spielhagen, R. F. & Mackensen, A. Upper ocean variability off NE Greenland (79°N) since the last glacial maximum reconstructed from stable isotopes in planktic foraminifer morphotypes. *Quat. Sci. Rev.* **265**, 107070 (2021).
33. Knies, J. et al. Nordic Seas polynyas and their role in preconditioning marine productivity during the Last Glacial Maximum. *Nat. Commun.* **9**, 3959–3910 (2018).
34. Bauch, H. A. et al. A multiproxy reconstruction of the evolution of deep and surface waters in the subarctic Nordic seas over the last 30,000yr. *Quat. Sci. Rev.* **20**, 659–678 (2001).
35. Thornalley, D. J. R. et al. A warm and poorly ventilated deep Arctic Mediterranean during the last glacial period. *Science* **349**, 706–710 (2015).
36. Muschitiello, F. et al. Deep-water circulation changes lead North Atlantic climate during deglaciation. *Nat. Commun.* **10**, 1272 (2019).
37. Brendryen, J., Haflidason, H., Yokoyama, Y., Haaga, K. A. & Hannisdal, B. Eurasian Ice Sheet collapse was a major source of Meltwater Pulse 1A 14,600 years ago. *Nat. Geosci.* **13**, 363–368 (2020).
38. Ascough, P., Cook, G. & Dugmore, A. Methodological approaches to determining the marine radiocarbon reservoir effect. *Prog. Phys. Geogr. Earth Environ.* **29**, 532–547 (2005).
39. Skinner, L. C. & Bard, E. Radiocarbon as a dating tool and tracer in paleoceanography. *Rev. Geophys.* **60**, e2020RG000720 (2022).
40. Østerhus, S. et al. Arctic Mediterranean exchanges: a consistent volume budget and trends in transports from two decades of observations. *Ocean Sci.* **15**, 379–399 (2019).
41. Lherminier, P. et al. The Atlantic Meridional Overturning Circulation and the subpolar gyre observed at the A25-OVIDE section in June 2002 and 2004. *Deep Sea Res. I* **57**, 1374–1391 (2010).
42. Våge, K. et al. The Irminger Gyre: Circulation, convection, and interannual variability. *Deep Sea Res. I Oceanogr. Res. Papers* **58**, 590–614 (2011).
43. Stern, J. V. & Lisiecki, L. E. North Atlantic circulation and reservoir age changes over the past 41,000 years. *Geophys. Res. Lett.* **40**, 3693–3697 (2013).
44. Ezat, M. M. et al. Ventilation history of Nordic Seas overflows during the last (de)glacial period revealed by species-specific benthic foraminiferal 14C dates. *Paleoceanography* **32**, 172–181 (2017).
45. Sikes, E. L., Samson, C. R., Guilderson, T. P. & Howard, W. R. Old radiocarbon ages in the southwest Pacific Ocean during the last glacial period and deglaciation. *Nature* **405**, 555–559 (2000).
46. Eiríksson, J., Larsen, G., Knudsen, K. L., Heinemeier, J. & Símonarson, L. A. Marine reservoir age variability and water mass distribution in the Iceland Sea. *Quat. Sci Rev.* **23**, 2247–2268 (2004).
47. Abbott, P. M., Griggs, A. J., Bourne, A. J., Chapman, M. R. & Davies, S. M. Tracing marine cryptotephras in the North Atlantic during the last glacial period: improving the North Atlantic marine tephrostratigraphic framework. *Quat. Sci. Rev.* **189**, 169–186 (2018).
48. Wastegård, S., Rasmussen, T. L., Kuijpers, A., Nielsen, T. & van Weering, T. C. E. Composition and origin of ash zones from Marine Isotope Stages 3 and 2 in the North Atlantic. *Quat. Sci. Rev.* **25**, 2409–2419 (2006).
49. Rutledal, S. et al. Tephra horizons identified in the western North Atlantic and Nordic Seas during the Last Glacial Period: Extending the marine tephra framework. *Quat. Sci. Rev.* **240**. https://doi.org/10.1016/j.quascirev.2020.106247 (2020).
50. Davies, S. M. et al. Identification of the Fugloyarbanki tephra in the NGRIP ice core: a key tie-point for marine and ice-core sequences during the last glacial period. *J. Quat. Sci.* **23**, 409–414 (2008).
51. Svensson, A. et al. A 60 000 year Greenland stratigraphic ice core chronology. *Clim. Past* 47–57 (2008).
52. Menviel, L., Timmermann, A., Friedrich, T. & England, M. H. Hindcasting the continuum of Dansgaard-Oeschger variability: mechanisms, patterns and timing. *Clim. Past* **4**, 63–77 (2014).
53. Goosse, H. et al. Description of the Earth system model of intermediate complexity LOVECLIM version 1.2. *Geosci. Model Dev.* **3**, 603–633 (2010).
54. Berger, A. Long-term variations of daily insolation and quaternary climatic changes. *J. Atmos. Sci.* **35**, 2362–2367 (1978).
55. Abe-Ouchi, A., Segawa, T. & Saito, F. Climatic Conditions for modelling the Northern Hemisphere ice sheets throughout the ice age cycle. *Clim. Past* **3**, 423–438 (2007).
56. Ahn, J. & Brook, E. J. Atmospheric CO_2 and climate on millennial time scales during the last glacial period. *Science* **322**, 83–85 (2008).
57. Martrat, B. et al. Four climate cycles of recurring deep and surface water destabilizations on the Iberian margin. *Science* **317**, 502–507 (2007).
58. Menviel, L. C., Skinner, L. C., Tarasov, L. & Tzedakis, P. C. An ice–climate oscillatory framework for Dansgaard–Oeschger cycles. *Nat. Rev. Earth Environ.* **1**, 677–693 (2020).

59. Smedsrud, L. H. et al. Nordic Seas Heat Loss, Atlantic Inflow, and Arctic Sea Ice cover over the last century. *Earth Space Sci. Open Arch.* **73**. https://doi.org/10.1002/essoar.10506171.2 (2021).
60. Menviel, L. et al. Poorly ventilated deep ocean at the Last Glacial Maximum inferred from carbon isotopes: a data-model comparison study. *Paleoceanography* **32**, 2–17 (2017).
61. Born, A., Imhof, M. A. & Stocker, T. F. An efficient surface energy–mass balance model for snow and ice. *Cryosphere* **13**, 1529–1546 (2019).
62. Zolles, T. & Born, A. Sensitivity of the Greenland surface mass and energy balance to uncertainties in key model parameters. *Cryosphere* **15**, 2917–2938 (2021).
63. Heaton, T. J. et al. Marine20-the marine radiocarbon age calibration curve (0–55,000 Cal BP). *Radiocarbon* **62**, 779–820 (2020).
64. Galbraith, E. D., Kwon, E. Y., Bianchi, D., Hain, M. P. & Sarmiento, J. L. The impact of atmospheric pCO2 on carbon isotope ratios of the atmosphere and ocean. *Glob. Biogeochem. Cycles* **29**, 307–324 (2015).
65. Schlosser, P. et al. The first trans-Arctic 14C section: comparison of the mean ages of the deep waters in the Eurasian and Canadian basins of the Arctic Ocean. *Nuclear Instr. Methods Phys. Res. B Beam Interact. Mater. Atoms* **123**, 431–437 (1997).
66. Östlund, H. G., Possnert, G. & Swift, J. H. Ventilation rate of the deep Arctic Ocean from carbon 14 data. *J. Geophys. Res.* **92**, 3769–3777 (1987).
67. Mangerud, J., Bondevik, S., Gulliksen, S., Karin Hufthammer, A. & Høisæter, T. Marine 14C reservoir ages for 19th century whales and molluscs from the North Atlantic. *Quat. Sci. Rev.* **25**, 3228–3245 (2006).
68. Cappelli, E. & Austin, W. E. N. Marine bivalve feeding strategies and radiocarbon ages in Northeast Atlantic coastal waters. *Radiocarbon* **62**, 107–125 (2020).
69. Wang, H., Legg, S. & Hallberg, R. The effect of Arctic freshwater pathways on North Atlantic convection and the Atlantic meridional overturning circulation. *J. Clim.* **31**, 5165–5188 (2018).
70. Hjort, C. A sea correction for East Greenland. *Geol. Fören. Stockh. Förh.* **95**, 132–134 (1973).
71. Chafik, L. & Rossby, T. Volume, heat, and freshwater divergences in the subpolar North Atlantic suggest the Nordic Seas as key to the state of the meridional overturning circulation. *Geophys. Res. Lett.* **46**, 4799–4808 (2019).
72. Hatun, H., Sando, A. B., Drange, H., Hansen, B. & Valdimarsson, H. Influence of the Atlantic subpolar gyre on the thermohaline circulation. *Science* **309**, 1841–1844 (2005).
73. Häkkinen, S., Rhines, P. B. & Worthen, D. L. Warm and saline events embedded in the meridional circulation of the northern North Atlantic. *J. Geophys. Res. Oceans* **116**. https://doi.org/10.1029/2010JC006275 (2011).
74. Dickson, R. R. et al. The Arctic Ocean response to the North Atlantic oscillation. *J. Clim.* **13**, 2671–2696 (2000).
75. Furevik, T., Mauritzen, C. & Ingvaldsen, R. in *Arctic Alpine Ecosystems and People in a Changing Environment* (eds Jon Børre Ørbæk, et al.) 123–146 (Springer, 2007).
76. Li, C. & Born, A. Coupled atmosphere-ice-ocean dynamics in Dansgaard-Oeschger events. *Quat. Sci. Rev.* **203**, 1–20 (2019).
77. Koul, V. et al. Unraveling the choice of the North Atlantic subpolar gyre index. *Sci. Rep.* **10**, 1005 (2020).
78. Asbjørnsen, H., Årthun, M., Skagseth, Ø. & Eldevik, T. Mechanisms of Ocean Heat Anomalies in the Norwegian Sea. *J. Geophys. Res. Oceans* **124**, 2908–2923 (2019).
79. Löfverström, M., Caballero, R., Nilsson, J. & Kleman, J. Evolution of the large-scale atmospheric circulation in response to changing ice sheets over the last glacial cycle. *Clim. Past* **10**, 1453–1471 (2014).
80. Merz, N., Raible, C. C. & Woollings, T. North Atlantic eddy-driven jet in interglacial and glacial winter climates. *J. Clim.* **28**, 3977–3997 (2015).
81. Nørgaard-Pedersen, N. et al. Arctic Ocean during the Last Glacial Maximum: Atlantic and polar domains of surface water mass distribution and ice cover. *Paleoceanography* **18**. https://doi.org/10.1029/2002PA000781 (2003).
82. Wacker, L., Fülöp, R. H., Hajdas, I., Molnár, M. & Rethemeyer, J. A novel approach to process carbonate samples for radiocarbon measurements with helium carrier gas. *Nuclear Instrum. Methods Phys. Res. B Beam Interact. Mater. Atoms* **294**, 214–217 (2013).
83. Hajdas, I., Bonani, G., Herrgesell Zimmerman, S., Mendelson, M. & Hemming, S. 14C ages of Ostracodes from Pleistocene Lake Sediments of the Western Great Basin, USA—results of progressive acid leaching. *Radiocarbon* **46**, 189–200 (2004).
84. Simstich, J., Sarnthein, M. & Erlenkeuser, H. Paired δ18O signals of Neogloboquadrina pachyderma (s) and Turborotalita quinqueloba show thermal stratification structure in Nordic Seas. *Marine Micropaleontol.* **48**, 107–125 (2003).
85. Greco, M., Jonkers, L., Kretschmer, K., Bijma, J. & Kucera, M. Depth habitat of the planktonic foraminifera Neogloboquadrina pachyderma in the northern high latitudes explained by sea-ice and chlorophyll concentrations. *Biogeosciences* **16**, 3425 (2019).
86. Reimer, P. J. et al. The Intcal20 Northern Hemisphere radiocarbon age calibration curve (0–55 Cal k BP). *Radiocarbon* **62**, 725–757 (2020).
87. Adolphi, F. et al. Connecting the Greenland ice-core and U/Th timescales via cosmogenic radionuclides: testing the synchroneity of Dansgaard–Oeschger events. *Clim. Past* **14**, 1755–1781 (2018).
88. Muscheler, R. et al. Testing and improving the IntCal20 calibration curve with independent records. *Radiocarbon* 1–16. https://doi.org/10.1017/RDC.2020.54 (2020).
89. Goosse, H. & Fichefet, T. Importance of ice-ocean interactions for the global ocean circulation: a model study. *J. Geophys. Res. Oceans* **104**, 23337–23355 (1999).
90. Opsteegh, J. D., Haarsma, R. J., Selten, F. M. & Kattenberg, A. ECBILT: a dynamic alternative to mixed boundary conditions in ocean models. *Tellus A Dyn. Meteorol. Oceanogr.* https://doi.org/10.3402/tellusa.v50i3.14524 (1998).
91. Brovkin, V. et al. Sensitivity of a coupled climate-carbon cycle model to large volcanic eruptions during the last millennium. *Tellus B Chem. Phys. Meteorol.* **62**, 674–681 (2010).
92. Mouchet, A. & François, L. M. Sensitivity of a global oceanic carbon cycle model to the circulation and to the fate of organic matter: preliminary results. *Phys. Chem. Earth* **21**, 511–516 (1996).
93. Menviel, L., Timmermann, A., Mouchet, A. & Timm, O. Climate and marine carbon cycle response to changes in the strength of the Southern Hemispheric westerlies. *Paleoceanography* **23**. https://doi.org/10.1029/2008PA001604 (2008).
94. Brady, E. C., Otto-Bliesner, B. L., Kay, J. E. & Rosenbloom, N. Sensitivity to Glacial Forcing in the CCSM4. *J. Clim.* **26**, 1901–1925 (2013).
95. Dee, D. P. et al. The ERA-Interim reanalysis: configuration and performance of the data assimilation system. *Quart. J. Royal Meteorol. Soc.* **137**, 553–597 (2011).
96. Holube, K. M., Zolles, T. & Born, A. Sources of uncertainty in Greenland surface mass balance in the 21st century. *Cryosphere* **16**, 315–331 (2022).
97. Amante, C. & Eakins, B. W. ETOPO1 1 arc-minute global relief model: procedures, data sources and analysis. NOAA Technical Memorandum NESDIS, NGDC-24, p 19 (NOAA National Centers for Environmental Information, 2009).
98. Simon, M. H. et al. Atlantic inflow into the southern Nordic Seas at the onset of the LGM promotes open-ocean conditions and Fennoscandian Ice Sheet growth. *SEANOE*. https://doi.org/10.17882/96079 (2023).
99. Schlitzer, R. Ocean Data View. www.odv.awi.de (2020).
100. Locarnini, R. A., A. V. Mishonov, O. K. Baranova, T. P. Boyer, M. M. Zweng, H. E. Garcia, J. R. Reagan, D. Seidov, K. Weathers, C. R. Paver, and I. Smolyar. World Ocean Atlas, Volume 1: Temperature., 52 (NOAA Atlas NESDIS 81, 2018).

Acknowledgements

We thank Dr. Lisa Griem and Dag Inge Blindheim for their help with sample preparation. We thank colleagues at the Department of Earth Science, UiB, Dr. Ulysses S. Ninnemann for stimulating discussions, and Dr. Willem van der Bilt for providing feedback on an earlier version of this manuscript regarding LGM ice sheets and moisture supply. We also thank the authors of the published Tephra and ^{14}C data for sharing and making their data open access. Finally, we would like to thank the R/V G.O. Sars and ice2ice GS16-204 cruise crew members for retrieving the material used in this study. The research leading to these results has received funding from the European Research Council under the European Community's Seventh Framework Program (FP7/2007-2013) / ERC grant agreement 610055 as part of the ice2ice project. LM acknowledges funding from the Australian Research Council, grant FT180100606. A.B. and T.Z. received funding from the Trond Mohn Foundation under the project "Modeling Englacial Layers and Tracers in Ice Sheets".

Author contributions

M.H.S. and S.R. designed the study. S.R. performed the MRA data collection and analysis. L.M. performed the LOVECLIM experiments. T.Z. and A.B. designed and performed the BESSI experiments. H.H. assisted with tephra analysis. S.M.P.B. supervised SR. T.M.D. supervised SR and acquired initial funding for this study. All authors discussed and interpreted the results. S.R. and M.H.S. wrote the manuscript with input from L.M., T.Z., H.H., A.B., S.M.P.B., and T.M.D. M.H.S. revised the manuscript. All authors reviewed the final manuscript.

Competing interests

The authors declare no competing interests.

Additional information

Supplementary information The online version contains supplementary material available at https://doi.org/10.1038/s43247-023-01032-9.

Correspondence and requests for materials should be addressed to Margit H. Simon.

Peer review information *Communications earth and environment* thanks Maciej Telesiński, Marit-Solveig Seidenkrantz and the other, anonymous, reviewers for their contribution to the peer review of this work. Primary Handling Editors: Sze Ling Ho and Clare Davis. A peer review file is available.